PHYSICAL REVIEW B **77**, 085411 (2008)

# Three-dimensional analysis of the geometrical rectifying properties of asymmetric metal-vacuum-metal junctions and extension for energy conversion

A. Mayer,[1,*] M. S. Chung,[2] B. L. Weiss,[3] N. M. Miskovsky,[4] and P. H. Cutler[4]

[1]*FUNDP - University of Namur, Rue de Bruxelles 61, B-5000 Namur, Belgium*

[2]*Department of Physics, University of Ulsan, Ulsan 680-749, Korea*

[3]*Department of Physics, 130 CAC, The Pennsylvania State University, Altoona, Pennsylvania 16601, USA*

[4]*Department of Physics, 104 Davey Laboratory, The Pennsylvania State University, University Park, Pennsylvania 16802, USA*

(Received 15 August 2007; published 8 February 2008)

We study the rectification properties of geometrically asymmetric metal-vacuum-metal junctions. In particular, we focus on systems in which the cathode metal supports a hemispherical protrusion. By using a transfer-matrix methodology to take account of three-dimensional aspects of the problem, we compute the forward and backward currents that flow in this device when it is subject to positive or negative external biases. These currents enable the calculation of the rectification properties of the device in the limit of quasistatic fields. We also determine the power this device could provide to an external load. We study in detail how these properties depend (i) on the magnitude of the bias established between the two metallic electrodes, (ii) on the separation between the two electrodes, (iii) on differences in the work function of the two metals, (iv) on differences in the temperature of the two metals, and (v) on the height of the protrusion. These calculations provide quantitative results for the use of these junctions as an energy converter and the efficiency with which the energy of incident radiation is being converted into a dc current and delivered to an external load.

DOI: 10.1103/PhysRevB.77.085411 PACS number(s): 85.30.Kk, 73.40.Ei, 79.70.+q, 03.65.Nk

## I. INTRODUCTION

Point-contact diodes were originally designed as metal-oxide-metal systems in which one of the metals is essentially flat while the other has an extended sharp tip.[1] Since their discovery, these diodes have been used for detection, rectification, and the frequency mixing of infrared radiation.[2–4] Fundamental applications of these devices have included the determination of the speed of light[5,6] or attempts to measure tunneling times.[7–11] They have also enabled accurate measurements of infrared frequencies.[12–14]

An explanation of the rectification properties of these devices in terms of their geometrical asymmetry was proposed by Lucas *et al.* in 1977.[15–17] The fact that an ac bias applied to these systems can induce currents with a strong dc component results from the difference in the potential barrier seen by electrons traveling in the forward versus the backward directions. The development of the scanning tunneling microscope in 1981 (Ref. 18) enabled well controlled experiments with metal-vacuum-metal asymmetric junctions. During this period it was determined that the cutoff frequency associated with the rectification properties of these junctions is inversely proportional to the spacing between the two metals. For a laser with 1.06 micron wavelength (0.28 THz frequency), the critical spacing associated with the cutoff of the rectification was measured to be around 25 Å.[9,10] Qualitatively, this cutoff of the rectification essentially arises because the bias reverses before the electron has been able to transit through the device.

Point-contact diodes are nowadays essentially used for the selective detection and mixing of infrared radiations. Current efforts aim at reducing the characteristic response times and improve the sensitivity of these systems.[19–21] The early theoretical work started by Lucas *et al.*[10,15–17] has not been pursued by recent computational techniques able to treat three-dimensional aspects of the potential barrier without the approximations usually introduced to both the shape of the barrier and the tunneling probabilities. Fundamental properties and potential applications of metal-vacuum-metal junctions exhibiting a geometrical asymmetry are still open to investigation. In particular, the conditions that would enable an efficient rectification in the visible range of the electromagnetic spectrum are still to be determined.

In this paper we investigate the rectification properties of metal-vacuum-metal systems in the limit where the external bias can be considered as quasistatic. We focus, in particular, on systems in which the cathode supports a hemispherical protrusion. The methodology used to compute the currents that flow in this device when it is subject to an external bias is presented in Sec. II. These currents enable the calculation of the rectification ratio of the device as well as the power this device could provide to an external load. In Sec. III, we study in detail the physics that govern these rectification properties by considering fixed geometrical and physical parameters. In Sec. IV, we study how these properties are affected by a variation of these parameters. In particular, we examine how they depend (i) on the magnitude of the bias established between the two metals, (ii) on the separation between the two metals, (iii) on differences in the work function of the two metals, (iv) on differences in the temperature of the two metals, and (v) on the height of the protrusion. These calculations were done in order to establish the validity of the model, although the dimensions and parameters for a practical structure have yet to be determined and are currently addressed. However, these calculations provide important insight into the use of these junctions as an energy converter, whereby some fraction of the energy of an incident radiation is being transferred via the dc current it induces in the junction to an external load.

 ©2008 The American Physical Society

## II. METHODOLOGY

The typical situation we consider in this paper is that in which two tungsten metals, delimited by flat parallel surfaces, are separated by a distance $D$. Initially, we assume $D=2$ nm. The bottom metal supports an hemispherical protrusion with a height of 1 nm and a radius of 0.5 nm. The system is subject to an external bias $V_{\mathrm{ext}}$, which is defined positive when the potential of the top metal is higher than that of the bottom metal and negative otherwise. We identify for convenience the $z$ axis with the vertical symmetry axis of the hemispherical tip. The surfaces of the bottom and top metals are defined as $z=0$ and $z=D$, respectively.

The potential energy relevant to electrons that tunnel through this device consists of three contributions: (i) the potential energy $E_{\mathrm{bias}}$ due to the external bias $V_{\mathrm{ext}}$, (ii) the image potential $E_{\mathrm{image}}$ that expresses the interaction of the tunneling electrons with the metallic elements, and (iii) the $E_F+W$ potential wells that characterize, in a jellium, picture the metallic elements. $E_F$ and $W$ refer, respectively, to the Fermi energy and to the work function of the two metals. For tungsten, we take $E_F=19.1$ eV and $W=4.5$ eV.

The first two contributions of this potential energy are calculated by using the finite-difference techniques presented in Appendix A of Ref. 22. For the first contribution, the boundary conditions are determined by the external bias $V_{\mathrm{ext}}$. More specifically, we take $V_{\mathrm{bias}}(\mathbf{r})=0$ as boundary conditions when $\mathbf{r}$ belongs to the bottom metallic elements and $V_{\mathrm{bias}}(\mathbf{r})=V_{\mathrm{ext}}$ when $\mathbf{r}$ belongs to the top metallic elements. We also take $V_{\mathrm{bias}}(\mathbf{r})=V_{\mathrm{ext}}z/D$ on the lateral limits of the simulation box, which is a convenient computational unit that is discussed in detail in Ref. 22. These limits are taken sufficiently far from the elements of interest in our system to make their impact on the potential-energy calculations negligible. After the finite-difference calculation of $V_{\mathrm{bias}}(\mathbf{r})$ in the entire system, the potential energy associated with the external bias is simply given by $E_{\mathrm{bias}}(\mathbf{r})=e[V_{\mathrm{ext}}-V_{\mathrm{bias}}(\mathbf{r})]$, where $e$ is the absolute value of the electronic charge. The constant $eV_{\mathrm{ext}}$ is added for the purpose of facilitating the interpretation of the potential-energy distributions shown hereafter and for consistency with our previous work.

For the second contribution, the boundary conditions on the metallic elements are given by $V_{\mathrm{met}}(\mathbf{r})=-V_e(\mathbf{r})$, where $V_e(\mathbf{r})=-\frac{1}{4\pi\epsilon_0}\frac{e}{|\mathbf{r}-\mathbf{r}_e|}$ is the potential associated with an electron at the position $\mathbf{r}_e$. We also take $V_{\mathrm{met}}(\mathbf{r})=0$ on the lateral limits of the simulation box. After the finite-difference calculation of $V_{\mathrm{met}}(\mathbf{r})$ in the entire system, the potential energy associated with the image potential of the electron at $\mathbf{r}_e$ is given by $E_{\mathrm{image}}(\mathbf{r}_e)=-eV_{\mathrm{met}}(\mathbf{r}_e)/2$, where the factor $1/2$ accounts for the fact we deal with a self-induced interaction.[23] These finite-difference calculations have to be repeated for every position $\mathbf{r}_e$ of interest in the system.

The potential energy one obtains by summing $E_{\mathrm{bias}}$, $E_{\mathrm{image}}$, and the $E_F+W$ potential wells when the external bias $V_{\mathrm{ext}}$ takes the value of 1 V is represented in Fig. 1. Since the physical situation is rotationally symmetric around the central $z$ axis of the tip, we represent only a vertical slice of this potential energy. The scattering calculations presented hereafter account for the three-dimensional aspect of the potential barrier.

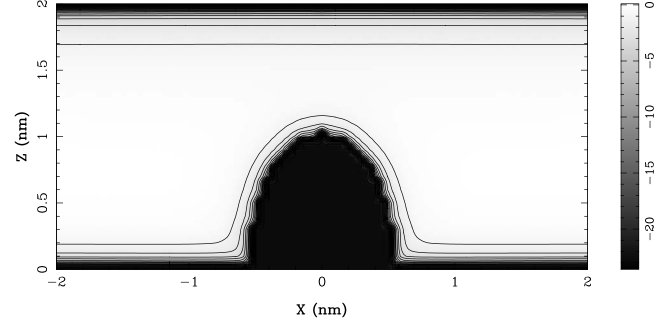


FIG. 1. Potential energy in the junction, for an external bias $V_{\mathrm{ext}}$ of 1 V. This result includes the contribution due to the 1 V external bias, the image potential, and the potential wells that characterize the metallic elements.

Once the potential energy is calculated, the next step consists of determining the currents that flow between the two metals. This is achieved by using the transfer-matrix methodology developed in Refs. 24–29. Using cylindrical coordinates, we expand the wave function in the bottom and top metals in terms of the basis states $\Psi^{\mathrm{I},\pm}_{m,j}(\mathbf{r})$ and $\Psi^{\mathrm{III},\pm}_{m,j}(\mathbf{r})$, which are defined by

$$\Psi^{\mathrm{I/III},\pm}_{m,j}(\rho,\phi,z)=\frac{RJ_m(k_{m,j}\rho)\exp(im\phi)}{\sqrt{2\int_0^R d\rho\rho[J_m(k_{m,j}\rho)]^2}}\times\exp\left(\pm i\sqrt{\frac{2m}{\hbar^2}(E-V_{\mathrm{I/III}})-k_{m,j}^2}z\right). \quad (1)$$

In this expression, "I" refers to the bottom metal and "III" to the top metal. The $J_m$ refer to the Bessel functions. The radial wave vectors $k_{m,j}$ are solutions of $J'_m(k_{m,j}R)=0$, with $R=2$ nm the radius of the cylinder in which we assume that the electrons are confined for the scattering calculation.[24] $E$ is the total energy of the electron. $V_{\mathrm{I}}=eV_{\mathrm{ext}}-W-E_F$ and $V_{\mathrm{III}}=-W-E_F$ refer to the potential energy in the bottom and top metals. The $\pm$ signs refer to the propagation direction relative to the $z$ axis.

Applying the transfer-matrix technique, one then obtains scattering solutions of the form

$$\Psi^{+}_{m,j}\overset{\mathbf{r}\in\text{region I}}{=}\Psi^{\mathrm{I},+}_{m,j}+\sum_{m',j'}S^{-+}_{(m',j'),(m,j)}\Psi^{\mathrm{I},-}_{m',j'}$$
$$\overset{\mathbf{r}\in\text{region III}}{=}\sum_{m',j'}S^{++}_{(m',j'),(m,j)}\Psi^{\mathrm{III},+}_{m',j'}, \quad (2)$$

$$\Psi^{-}_{m,j}\overset{\mathbf{r}\in\text{region I}}{=}\sum_{m',j'}S^{--}_{(m',j'),(m,j)}\Psi^{\mathrm{I},-}_{m',j'}$$
$$\overset{\mathbf{r}\in\text{region III}}{=}\Psi^{\mathrm{III},-}_{m,j}+\sum_{m',j'}S^{+-}_{(m',j'),(m,j)}\Psi^{\mathrm{III},+}_{m',j'}, \quad (3)$$

corresponding to single incident states $\Psi^{\mathrm{I},+}_{m,j}$ and $\Psi^{\mathrm{III},-}_{m,j}$ in the bottom and top metals for a given value of the energy $E$.

Total current densities result from the contribution of every solution associated with a propagative state in the region of incidence. Therefore, the upward current from metal I to metal III is given by

$$I^{+} = \frac{2e}{h}\int_{V_{\mathrm{I}}}^{+\infty} f_{\mathrm{I}}(E)[1-f_{\mathrm{III}}(E)] \times \sum_{(m',j'),(m,j)} \frac{v_{\mathrm{III},(m',j')}}{v_{\mathrm{I},(m,j)}} |S^{++}_{(m',j'),(m,j)}|^2 dE, \quad (4)$$

while the downward current from metal III to metal I is given by

$$I^{-} = \frac{2e}{h}\int_{V_{\mathrm{III}}}^{+\infty} f_{\mathrm{III}}(E)[1-f_{\mathrm{I}}(E)] \times \sum_{(m',j'),(m,j)} \frac{v_{\mathrm{I},(m',j')}}{v_{\mathrm{III},(m,j)}} |S^{--}_{(m',j'),(m,j)}|^2 dE. \quad (5)$$

In these expressions, $v_{\mathrm{I/III},(m,j)}=\frac{\hbar}{m}\sqrt{\frac{2m}{\hbar^2}(E-V_{\mathrm{I/III}})-k^2_{m,j}}$ refers to the group velocity in the bottom and top metals. $f_{\mathrm{I}}(E)=1/\{\exp[(E-\mu_{\mathrm{I}})/kT]+1\}$ and $f_{\mathrm{III}}(E)=1/\{\exp[(E-\mu_{\mathrm{III}})/kT]+1\}$ are the Fermi factors of the two metals, with $\mu_{\mathrm{I}}=eV_{\mathrm{ext}}-W$ and $\mu_{\mathrm{III}}=-W$ their chemical potential, $T$ the temperature and $k$ the Boltzmann constant. We initially assume $T=300$ K. The summation in these integrals must include only propagative states.[30]

For a positive external bias, the forward current will be given by $I_{\mathrm{forward}}=I^{+}-I^{-}$. For a negative external bias, the backward current will be given by $I_{\mathrm{backward}}=I^{-}-I^{+}$. The rectification ratio corresponding to an external bias with amplitude $V_{\mathrm{ext}}$ is defined as $\mathrm{Rect}=I_{\mathrm{forward}}/I_{\mathrm{backward}}$. The rectification ratio quantifies the capacity of the junction to provide a forward current when subject to a bias with alternating polarity. Considering a full cycle in which the external bias alternates between $+V_{\mathrm{ext}}$ and $-V_{\mathrm{ext}}$, the mean power the device can provide to an external load is given by $\langle P\rangle=\frac{1}{2}V_{\mathrm{ext}}(I_{\mathrm{forward}}-I_{\mathrm{backward}})=\frac{1}{2}V_{\mathrm{ext}}I_{\mathrm{forward}}(1-1/\mathrm{Rect})$. In order to maximize this quantity, one must therefore seek conditions that maximize both $I_{\mathrm{forward}}$ and the rectification ratio Rect.

This definition of the mean power $\langle P\rangle$ the device could provide to an external circuit only makes sense for conditions where the time taken by electrons in order to cross the device is significantly smaller than the frequency at which the external bias $V_{\mathrm{ext}}$ oscillates. For the device represented in Fig. 1, the time $t_{\mathrm{tot}}$ typically taken by electrons in order to cross the part of the junction that is subject to the external field consists of (i) the time $t_{\mathrm{tunnel}}$ required to tunnel through the classically forbidden part of the surface barrier, and (ii) the time $t_{\mathrm{propag}}$ required to propagate classically in vacuum from the surface barrier to the anode. The tunneling time $t_{\mathrm{tunnel}}$ is evaluated by assuming that electrons propagate at the Fermi velocity in the classically forbidden region.[10] This choice of the Fermi velocity is approximately that determined in one-dimensional wave-packet simulations by Nguyen *et al.*[9] and Hartman.[11] The propagation time $t_{\mathrm{propag}}$ is then calculated according to classical mechanics. These two contributions are evaluated for electrons that propagate along the central $z$ axis of the system at the Fermi level of the bottom metal. For the situation depicted in Fig. 1, the traversal time $t_{\mathrm{tot}}$ takes the value of 0.5 fs, which corresponds to a cutoff frequency $\nu_{\mathrm{cutoff}}=\frac{1}{2t_{\mathrm{tot}}}$ of 1 THz (electromagnetic wavelength of 300 nm in the ultraviolet).[10] We will check systematically, for each new value of the external bias $V_{\mathrm{ext}}$ or spacing $D$, the cutoff frequency that applies to our assumption that the external field can be considered as quasistatic. For frequencies that exceed this limit, photon absorption or emission processes must be taken into account and the formalism presented in Refs. 4 and 28 for dealing with oscillating barriers shall be used.

## III. APPLICATION: RECTIFICATION PROPERTIES OF A JUNCTION WITH GIVEN GEOMETRICAL AND PHYSICAL PARAMETERS

In this section we consider the physics that governs the rectification properties of a junction with given geometrical and physical parameters. In particular, we focus on the situation depicted in Fig. 1 in which the external bias $V_{\mathrm{ext}}$ takes the value of 1 V. These small values of both the spacing $D$ (2 nm) and the external bias $V_{\mathrm{ext}}$ (1 V) aim at a better illustration of the physical processes that occur in the junction. Larger and more practical values for $D$ and $V_{\mathrm{ext}}$ are considered in Sec. IV.

In order to better understand the results presented hereafter, we show in the left part of Fig. 2 a vertical section of the potential energy given in Fig. 1. This figure provides the potential energy relevant to an electron propagating along the $z$ axis when the external bias $V_{\mathrm{ext}}$ takes the value of 1 V. The Fermi level of electrons in the bottom metal is at $eV_{\mathrm{ext}}-W=-3.5$ eV, while the Fermi level of electrons in the top metal is at $-W=-4.5$ eV. The right part of Fig. 2 shows the total-energy distribution of the forward current.

The forward current $I_{\mathrm{forward}}=I^{+}-I^{-}$ is $2.53\times10^{-12}$ A. The downward current $I^{-}$ turns out to be 16 orders of magnitude smaller than the upward current $I^{+}$ so that the forward current $I_{\mathrm{forward}}$ is dominated by the electrons that tunnel from the bottom to the top metal. To explain this behavior and the shape of the total-energy distribution of Fig. 2, we note that electronic transmission between the two metals is only significant when there are (i) occupied electronic states in the metal from which electrons tunnel and (ii) empty electronic states in the metal in which electrons arrive. When $V_{\mathrm{ext}}$ is positive, these two conditions are essentially met for electrons tunneling upwards, in the energy window delimited by the Fermi levels of the two metals. For an external bias of 1 V, the Fermi level of the bottom metal is 1 eV higher than that of the top metal. Conditions are therefore appropriate for a preferential tunneling of electrons from the bottom to the top metal, while there are few unoccupied electronic states in the bottom metal to accommodate electrons wanting to tunnel downwards from the top to the bottom metal (at characteristic energies close to the Fermi energy of the top metal). This explains the fact $I^{-}$ is smaller by 16 orders of magnitude than $I^{+}$. Besides these issues, the probability electrons have to cross the potential barrier constitutes another important factor for explaining the energy distribution of Fig. 2. This

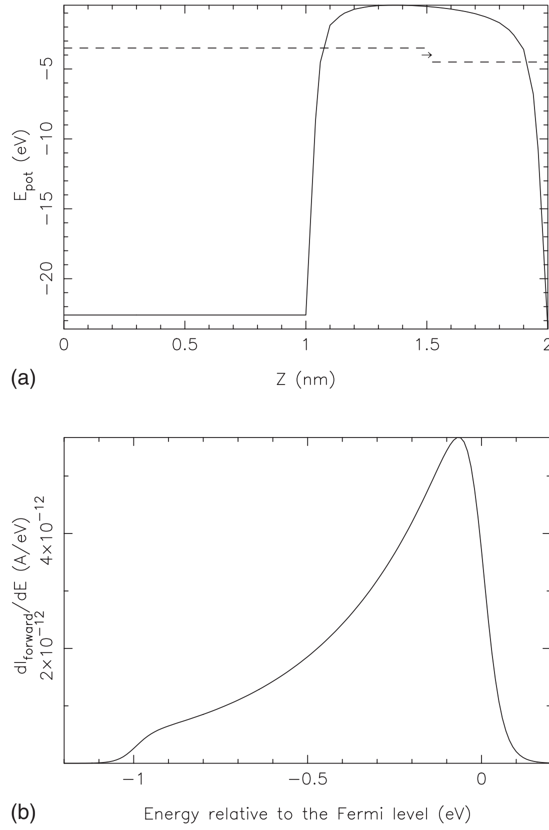


FIG. 2. (a) Potential energy along the $z$ axis, for an external bias $V_{ext}$ of 1 V. The Fermi level in the bottom and top metals is indicated by dashed lines. The arrow indicates the direction of the net electronic current. (b) Total-energy distribution of the forward current. The energy is represented relative to the Fermi level of the bottom metal.

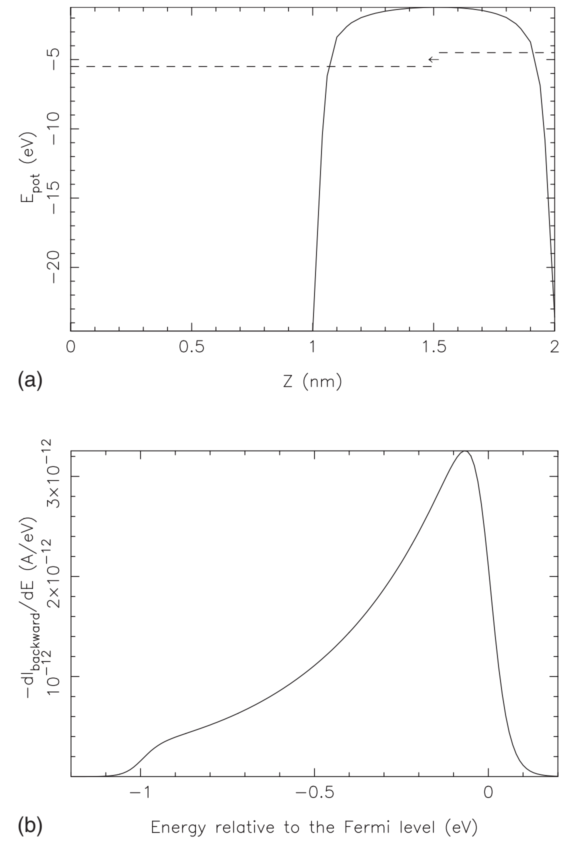


FIG. 3. (a) Potential energy along the $z$ axis, for an external bias $V_{ext}$ of −1 V. The Fermi level in the bottom and top metals is indicated by dashed lines. The arrow indicates the direction of the net electronic current. (b) Total-energy distribution of the backward current. The energy is represented relative to the Fermi level of the top metal.

transmission probability increases with the electron energy. This explains why the energy distributions of actually both the upward and downward currents take their maximal value close to the upper limit of the energy window where these currents are significant.

If we change the external bias $V_{ext}$ from a value of 1 V to −1 V, we create a situation in which electrons flow preferentially from the top to the bottom metal. We represented in the left part of Fig. 3 a vertical section of the potential energy in the junction. This figure provides the potential energy relevant to an electron propagating along the $z$ axis when the external bias $V_{ext}$ takes the value of −1 V. The Fermi level of electrons in the bottom metal is at $eV_{ext}-W=-5.5$ eV, while the Fermi level of electrons in the top metal is at $-W=-4.5$ eV. The right part of Fig. 3 shows the total-energy distribution of the backward current.

The backward current $I_{backward}=I^{-}-I^{+}$ is $1.48\times10^{-12}$ A. The upward current $I^{+}$ is now 16 orders of magnitude smaller than the downward current $I^{-}$, so that the backward current $I_{backward}$ obtained in this reverse bias condition is dominated by the electrons that tunnel from the top to the bottom metal. This behavior is explained this time by the unavailability of free electronic states for electrons wanting to tunnel upwards from the bottom to the top metal. With an external bias of −1 V, the Fermi level of the top metal is indeed 1 eV above that of the bottom metal. Preferential tunneling occurs therefore in the downwards direction, from the filled electronic states of the top metal to the unoccupied electronic states of the bottom metal, in an energy window delimited by the Fermi levels of the two metals. The fact the transmission probability increases with the electron energy explains why the energy distributions of both the upward and downward currents exhibits a maximum close to the upper limit of these distributions.

With the 1 V external bias, we had achieved a forward current of $2.53\times10^{-12}$ A. The backward current with a −1 V external bias is, however, smaller, $1.48\times10^{-12}$ A. For the same magnitude of the external bias, the forward current when the bias is positive is thus higher than the backward current when the bias is negative. The reason for this difference is due to the fact the potential energy seen by an electron propagating upwards at the Fermi level of the bottom metal in forward-bias conditions is different from the potential energy seen by an electron propagating downwards at the Fermi level of the top metal in reverse-bias conditions. This difference in the barrier encountered by the tunneling electrons explains the difference between the forward and backward currents. This difference in the currents has a purely geometrical origin. Another way to explain the difference

between $I_{\text{forward}}$ and $I_{\text{backward}}$ is to point out the fact that the elongated aspect of the tip is favorable to a forward current (when the bias is positive), while there is no field enhancement on the top metal to increase the backward current.

The rectification ratio of the junction is given by the ratio between the forward current $I_{\text{forward}}$ with a bias of 1 V and the backward current $I_{\text{backward}}$ with a bias of −1 V. For these conditions, the ratio is 1.71. This result is significant. It implies that an alternating field (possibly that of an electromagnetic radiation) will induce a net electronic current from the bottom to the top metal. This device may therefore act as an energy converter, transforming the energy of the radiation into that of a dc electronic current. The origin of that conversion is not material (the two metals are identical), but purely geometrical. The mean power this junction could supply to an external load because of this rectification behavior is $\langle P\rangle = \frac{1}{2}V_{\text{ext}}(I_{\text{forward}} - I_{\text{backward}}) = 0.5\times 10^{-12}$ W. This value, which holds for frequencies up to 1 THz, could be increased by seeking conditions in which the forward current is larger. Emissions around 1 mA are indeed routinely obtained by using elongated structures. By increasing the density of emitters and by focusing the electromagnetic radiation, it is conceivable to raise the power to values that are more appropriate for applications. We will study in the next section how these properties change with the external bias, the separation between the two metals, their work function, their temperature, and finally, the height of the protrusion.

## IV. APPLICATION: RECTIFICATION PROPERTIES OF THE JUNCTION FOR VARIOUS GEOMETRICAL AND PHYSICAL PARAMETERS

We investigate in this section how the rectification properties of the junction depends on the voltage, the geometry of the device, and the physical parameters of the two metals. This study will show that higher rectification ratios can be achieved by tuning the magnitude of the external bias to an optimal value (which depends on the geometry of the device), by increasing the distance between the two metals, by considering metals with different work functions, by increasing the temperature of the bottom metal, or by increasing the height of the emitter. We will also consider the power this device can provide to an external load. This study aims at establishing these points in a more quantitative way by using the transfer-matrix methodology in order to account for three-dimensional aspects of the problem.

### A. Dependence of the rectification properties on the external bias

We investigate in this section how the magnitude of the external bias affects the rectification ratio of the junction. We consider again the junction depicted in Fig. 1, which corresponds to a metal separation $D$ of 2 nm. We let the external bias $V_{\text{ext}}$ vary between 0 and 10 V, considering for each case positive and negative polarities. We realize that these spacing and voltage values are unrealistic for a real operating device. Nevertheless the physics of the operation is valid and would scale with the size of the device. They hence demonstrate the

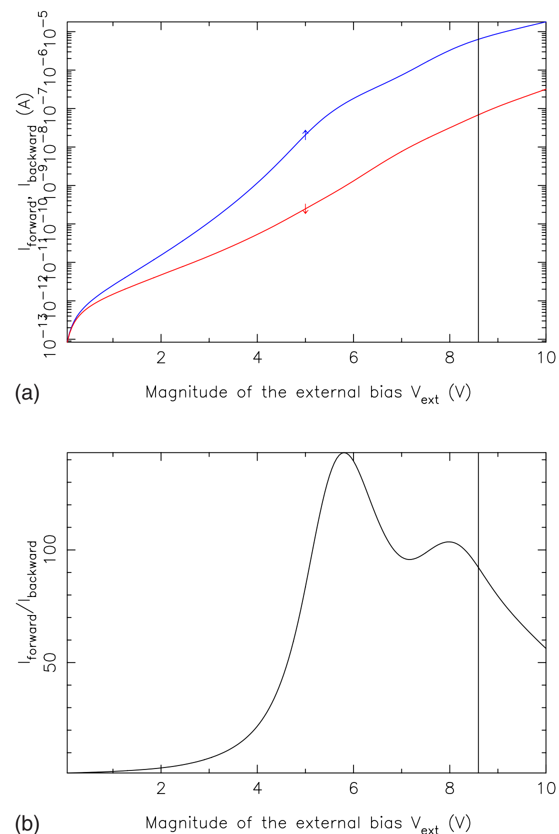


FIG. 4. (Color online) (a) Forward (curve indicated by an upward arrow) and backward (curve indicated by a downward arrow) currents as a function of the magnitude of the external bias $V_{\text{ext}}$. (b) Rectification ratio of the junction as a function of the magnitude of the external bias $V_{\text{ext}}$. The spacing $D$ between the two metals is 2 nm. The vertical line indicates the voltage at which the tunneling part of the barrier, for electrons propagating along the $z$ axis at the Fermi level of the bottom metal, disappears.

basic physics that would be associated with these more realistic structures.

The forward currents $I_{\text{forward}}$ we obtain for positive $+V_{\text{ext}}$ external bias and the backward currents $I_{\text{backward}}$ we obtain for negative $-V_{\text{ext}}$ external bias are represented in Fig. 4. This figure also represents the rectification ratio of the junction. The vertical line indicates the voltage at which the tunneling part of the surface barrier, for electrons propagating along the $z$ axis at the Fermi level of the bottom metal, disappears. A realistic cathode would not sustain currents corresponding to voltages much higher than this limit because of overheating effects.

The results of Fig. 4 show that the forward current is always greater than the backward current. The ratio between these two quantities reaches a maximum for a value of the external bias around 5.8 V (rectification ratio of 143.2). There is therefore an optimal bias for the rectification ratio. The forward and backward currents do not increase at a steady rate. Increased emission is indeed expected when the energy of the tunneling electrons satisfies standing-wave conditions between the two metals, that is, resonance conditions. These effects, which explain the oscillations in the

rectification ratio, are only significant when the separation $D$ between the two metals is of the order of a few nanometers. As will be demonstrated later, these oscillations tend to get closer to each other as the distance $D$ between the two metals is increased. They would not be observable at macroscopic distances between the two metals. At microscopic distances however, these oscillations could be used to detect modifications in the gap spacing or in the external bias because of the sudden variations these modifications would induce on the currents.

The results presented so far are fully consistent with those achieved in previous work by Lucas *et al.*[15–17] Their results indicate also an optimal rectification ratio at a bias of the order of 6 V for similar separations between the tip and the anode. A significant difference in the methodology consists of the fact we evaluate the transmission probability of the different electronic states in the two metals by a transfer-matrix methodology, which accounts for the three-dimensional dependence of the potential energy. In contrast, the results achieved by Lucas *et al.* rely on the JWKB approximation,[31] which is essentially a one-dimensional approach that does not account for interference effects in the barrier. These interference effects are accounted for by our methodology. They are manifested by the oscillations in the results shown in Fig. 4.

The mean power $\langle P \rangle$ the device can provide to an external load is directly proportional to the forward current, which increases with the external bias. As the external bias increases, the classically forbidden part of the surface barrier tends to disappear and the characteristic propagation time in the junction tends to be essentially determined by the time electrons take to propagate classically between the apex of the protrusion and the anode. At the voltage at which the tunneling part of the surface barrier disappears (8.6 V), $\langle P \rangle$ takes the value of $2.7 \times 10^{-5}$ W. The cutoff frequency at this voltage is 0.4 THz, which corresponds to a radiation wavelength of 750 nm (near infrared). In rectifying optical frequencies, the potential barrier will change several times by the time electrons propagate from the apex of the tip to the anode. One has therefore to apply the techniques presented in Ref. 28 in order to account for the photon absorption and emission processes. The current paper aims at providing results corresponding to the limit of quasistatic fields ($\omega \to 0$). Future work will address this rectification problem from the point of view of an oscillating barrier.

### B. Dependence of the rectification properties on the spacing between the two metals

It is interesting to compare the results obtained so far with the spacing $D$ of 2 nm between the two metals with those obtained by considering $D=4$ nm. The forward and backward currents, as well as the rectification ratio, one obtains by varying the magnitude of the external bias between 0 and 20 V are represented in Fig. 5. We also indicate by a vertical line the voltage at which the tunneling part of the surface barrier, for electrons propagating along the $z$ axis at the Fermi level of the bottom metal, disappears.

The results are of a similar nature as those obtained with the 2 nm spacing. The increased distance between the two metals enhances the difference between the forward current (which benefits from the field enhancement at the tip) and the backward current (for which no field enhancement applies). An optimal rectification factor is achieved around 5.9 V (rectification factor of 25 800). The oscillations in the rectification ratio are closer than in the previous case. Because of the increased distance between the two metals, standing-wave conditions are indeed encountered at lower energies and with smaller energy separations than with the spacing of 2 nm. The number of these oscillations actually increases regularly with the spacing between the two metals.

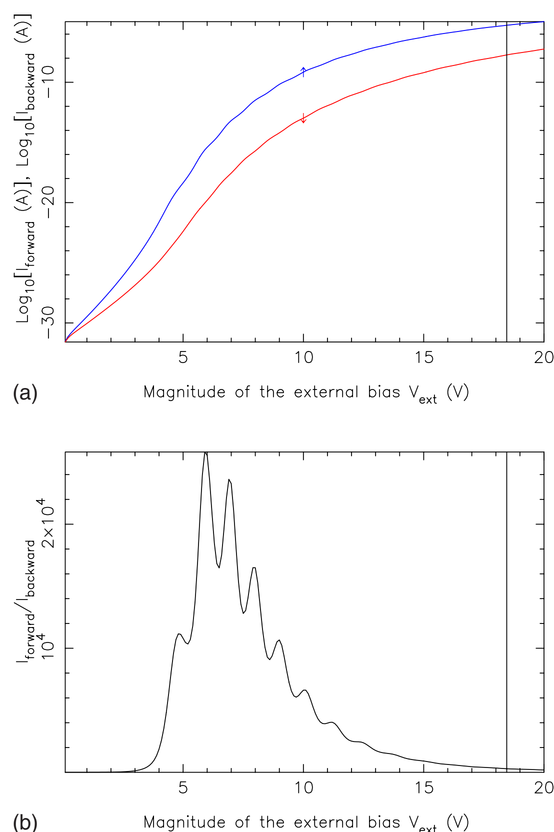


FIG. 5. (Color online) (a) Forward (curve indicated by an upward arrow) and backward (curve indicated by a downward arrow) currents as a function of the magnitude of the external bias $V_{ext}$. (b) Rectification ratio of the junction as a function of the magnitude of the external bias $V_{ext}$. The spacing $D$ between the two metals is 4 nm. The vertical line indicates the voltage at which the tunneling part of the barrier, for electrons propagating along the $z$ axis at the Fermi level of the bottom metal, disappears.

Considering the voltage at which the tunneling part of the surface barrier disappears (18.4 V), we obtain $5.2 \times 10^{-5}$ W as the value for the mean power $\langle P \rangle$ this junction could provide to an external load. This value is approximately twice the value of $2.7 \times 10^{-5}$ W obtained at 8.6 V when considering a spacing $D$ of 2 nm. When increasing the spacing $D$ by maintaining the macroscopic field $V_{ext}/D$ constant so that $I_{forward}$ keeps essentially unaffected, the mean power $\langle P \rangle$ must indeed increase proportionally to $D$. The time electrons take to cross the device increases however, also with $D$, so that the cutoff frequency is reduced. The cutoff frequency

corresponding to this voltage of 18.4 V is 0.2 THz (infrared), which is indeed smaller than the value of 0.4 THz achieved when $D=2$ nm. These cutoff frequencies are determined by the classical propagation time of electrons between the surface barrier and the anode. At lower voltages, considering that electrons propagate at the Fermi velocity in the tunneling barrier, we achieve cutoff frequencies that go up to 0.42 THz (red-infrared) at the limit where $V_{ext} \simeq 0$.

### C. Dependence of the rectification properties on the work function of the two metals

Besides geometrical asymmetries, one can also investigate the effect of an asymmetry in the material properties of the two metals. We have considered so far tungsten, whose work function is 4.5 eV. We will reduce artificially the work function of either the bottom or the top metal to the value of 3.5 eV and observe the consequences on the rectification properties of the junction. This reduction of the work function could be due to a choice of material or adsorbed species on the surface of the metals.

In situations in which the work functions $W_I$ and $W_{III}$ of the two metals are different, the equilibration of the Fermi levels results in an intrinsic bias $(W_I - W_{III})/e$ in the junction, which exists independently of the bias $V_{ext}$ applied externally to the junction. The bias effectively present in the junction is therefore given by

$$V_{tot} = \frac{W_I - W_{III}}{e} + V_{ext}. \quad (6)$$

This contribution of $\frac{W_I - W_{III}}{e}$ to the bias present in the junction must be taken into account in exactly the same way as $V_{ext}$ in the potential-energy and transfer-matrix calculations.

Reducing the work function $W_I$ of the bottom metal tends to increase the forward current. On the other hand, because of Eq. (6), it also reduces the bias $V_{tot}$ effectively present in the junction. This reduction of $V_{tot}$ corresponds (i) to a reduction of the field applied on the bottom metal (this effect is not sufficient, however, to prevent the forward current from increasing because of the reduction in the work function), and (ii) to an increase of the field applied to the top metal (which leads to an increase of the backward current). This second effect becomes less significant as the spacing $D$ between the two metals increases. The correction $\frac{W_I - W_{III}}{eD}$ to the effective macroscopic field decreases as $D \to \infty$.

In a similar way, reducing the work function $W_{III}$ of the top metal tends to increase the backward current. On the other hand, because of Eq. (6), it also increases the bias $V_{tot}$ effectively present in the junction. This increase of $V_{tot}$ corresponds (i) to a reduction of the field applied on the top metal (again, this effect is not sufficient to prevent the backward current from increasing), and (ii) to an increase of the field applied to the bottom metal (which leads to an increase of the forward current). Here too, this second effect becomes less significant as the spacing $D$ between the two metals tends to infinity. In order to reduce effects that are only significant when $D$ is small, we considered a spacing $D$ of 4 nm and observed the consequences of a modification in the work function of the two metals.

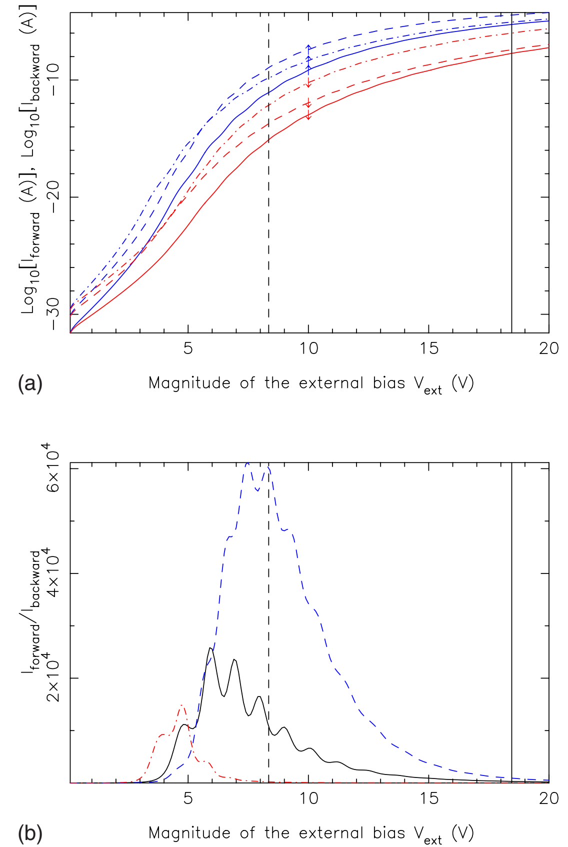


FIG. 6. (Color online) (a) Forward (curves indicated by an upward arrow) and backward (curves indicated by a downward arrow) currents as a function of the magnitude of the external bias $V_{ext}$. (b) Rectification ratio of the junction as a function of the magnitude of the external bias $V_{ext}$. The work function of the bottom and top metals is 4.5 and 4.5 eV (solid), 3.5 and 4.5 eV (dashed), and 4.5 and 3.5 eV (dot-dashed), respectively. The spacing $D$ between the two metals is 4 nm. The vertical lines indicate the voltage at which the tunneling part of the barrier, for electrons propagating along the $z$ axis at the Fermi level of the bottom metal, disappears.

The results are presented in Fig. 6. The figure actually presents the forward and backward currents as well as the rectification ratio one obtains when the work function of either the bottom or the top metal is decreased to 3.5 eV. We also indicate the voltage at which the tunneling part of the surface barrier, for electrons traveling on the $z$ axis at the Fermi level of the bottom metal, disappears. In each case, one observes an increase of both the forward and backward currents in agreement with the explanations provided in the previous paragraph. For a given spacing $D$, and because of Eq. (6), the effects associated with the modification of the bias effectively present in the junction are only significant when the external bias $V_{ext}$ is small. The effects are essentially the increase of $I_{backward}$ when $W_I$ is decreased and the increase of $I_{forward}$ when $W_{III}$ is decreased. When the external voltage $V_{ext}$ becomes more significant, the effects directly associated with the reduction of the work function dominate the process. Reducing $W_I$ then results essentially in an increase of the forward current and in higher values of the rectification ratio. Similarly, reducing $W_{III}$ results essentially

in an increase of the backward current and in lower values of the rectification ratio.

The mean power $\langle P \rangle$ the junction can supply to an external load is proportional to the forward current, which increases when the work function $W_{\rm I}$ of the bottom metal is reduced. For a given voltage, one hence obtains a higher forward current and a higher mean power when $W_{\rm I}$=3.5 eV. Another consequence of this increase of the forward current is that the critical point at which the tunneling part of the surface barrier disappears is reached at a lower voltage. With $W_{\rm I}$=3.5 eV, this critical point is reached at $V_{\rm ext}$=8.4 V and $\langle P \rangle$ takes the value of $5.6\times10^{-9}$ W. The corresponding cutoff frequency is 0.1 THz (infrared). In the original situation in which $W_{\rm I}$=4.5 eV, the bias at which the tunneling part of the surface barrier disappears is 18.4 V and the forward current is actually larger, so that the mean power is $5.2\times10^{-5}$ W.

### D. Dependence of the rectification properties on the temperature of the two metals

Besides geometric and material properties, temperature constitutes another possible source of asymmetry in the junction. We increased the temperature of either the bottom or the top metal from 300 K to 800, 1300, and 1800 K. These simulations were achieved for a spacing $D$ of 4 nm between the two metals.

Increasing the temperature $T_{\rm I}$ of the bottom metal results essentially in an increase of the forward current. Increasing the temperature excites electrons to higher energy levels, for which the probability to escape to the vacuum is larger. This increase in the forward current results in a higher rectification ratio. In a similar way, increasing the temperature $T_{\rm III}$ of the top metal results essentially in an increase of the backward current, which in turn reduces the rectification ratio.

We present in Fig. 7 the forward and backward currents as well as the rectification ratio obtained by increasing the temperature of either the top or the bottom metal. These results are well explained by the previous comments. We note that increasing the temperature of the bottom metal from 300 to 800 K leads to a magnification of the rectification ratio that is as large as that observed by reducing $W_{\rm I}$ from 4.5 to 3.5 eV.

The mean power $\langle P \rangle$ the junction can provide to an external load takes its highest value in the case where the temperature $T_{\rm I}$ of the bottom metal is 1800 K. At the bias at which the tunneling part of the potential barrier disappears (18.4 V), this mean power is $6.1\times10^{-5}$ W. The cutoff frequency is 0.2 THz. This maximal value for the mean power $\langle P \rangle$ is actually comparable with that determined when $T_{\rm I}$ =300 K ($5.2\times10^{-5}$ W).

### E. Dependence of the rectification properties on the height of the protrusion

We finally simulate situations in which the hemispherical protrusion is supported by a cylindrical body. We actually increase the length of this cylindrical body from 0 to 3 nm and study the impact of these modifications on the rectification properties of the junction. We assume the cylindrical body and the hemispherical protrusion have a radius of 1 nm. We also increase the spacing $D$ between the two metals to 6 nm. We show in Fig. 8 the potential energy corresponding to the limiting cases where the height of the protrusion, which consists of the cylindrical body and the hemispherical cap, is 1 and 4 nm.

The forward and backward currents, as well as the rectification ratio one obtains when the height of the protrusion takes the value of 1, 2, 3, and 4 nm are depicted in Fig. 9. These calculations are done for an external bias $V_{\rm ext}$ ranging between 0 and 20 V. We assume, as previously, that the metals are made of tungsten and that the temperature $T$ is 300 K. The figure reveals that both the forward and the backward currents increase with the height of the tip. The increase of the forward current is due to the increase of the field-enhancement factor of the tip. The increase of the backward current is due to the reduction of the distance between the

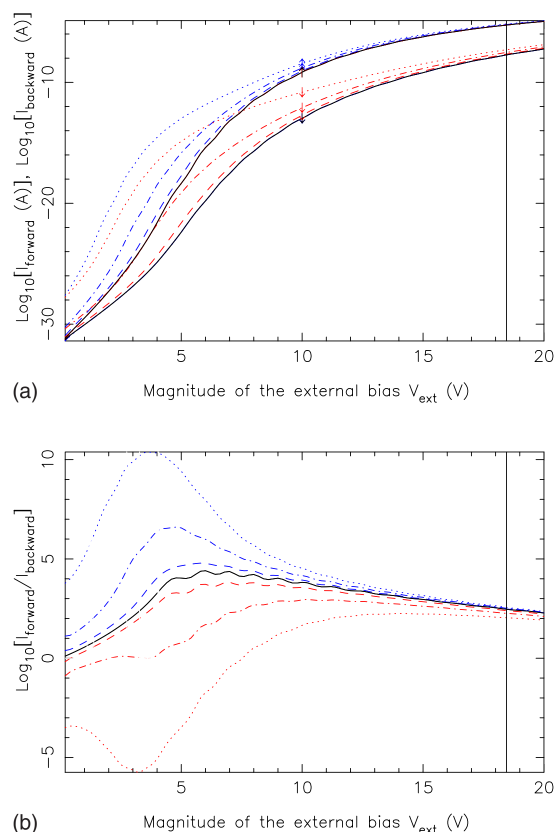


FIG. 7. (Color online) (a) Forward (curves indicated by an upward arrow) and backward (curves indicated by a downward arrow) currents as a function of the magnitude of the external bias $V_{\rm ext}$. (b) Rectification ratio of the junction as a function of the magnitude of the external bias $V_{\rm ext}$. The temperature of the bottom and top metals are, respectively, 300 and 300 K (solid), 800 and 300 K (top, dashed), 1300 and 300 K (top, dot-dashed), 1800 and 300 K (top, dotted), 300 and 800 K (bottom, dashed), 300 and 1300 K (bottom, dot-dashed), and 300 and 1800 K (bottom, dotted). The spacing $D$ between the two metals is 4 nm. The vertical line indicates the voltage at which the tunneling part of the barrier, for electrons propagating along the $z$ axis at the Fermi level of the bottom metal, disappears.

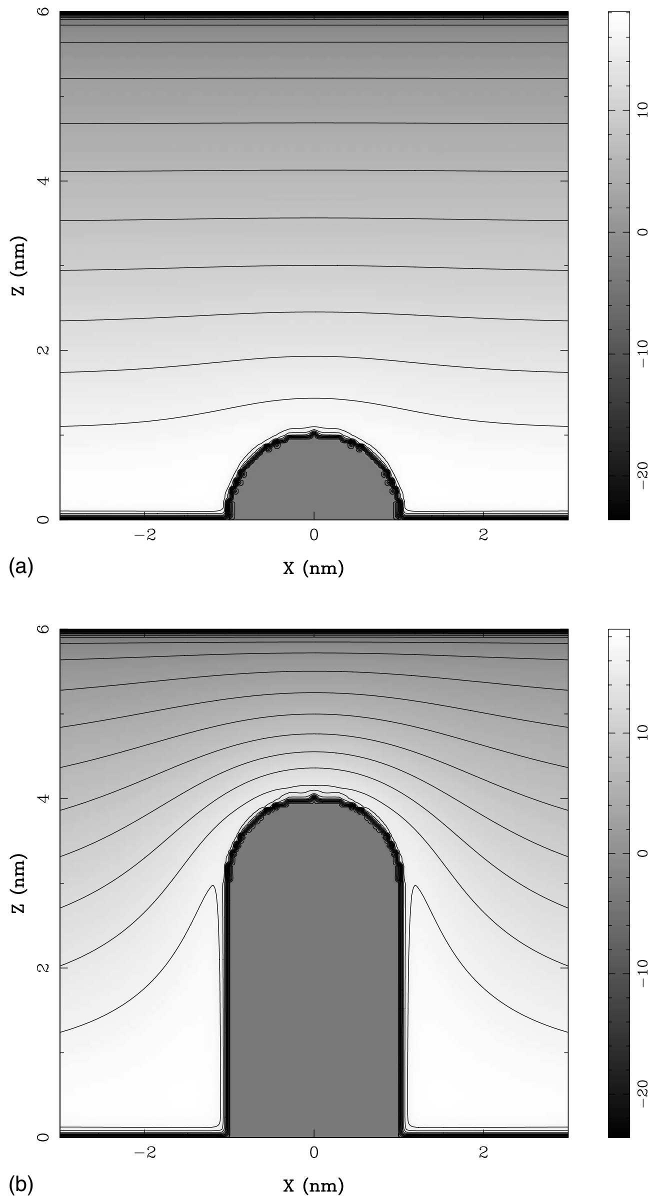


FIG. 8. Potential energy in the junction, for an external bias $V_{ext}$ of 20 V and a spacing $D$ between the two metals of 6 nm. The bottom metal supports a protrusion that consists of (i) a cylindrical body with a radius of 1 nm and a height of, respectively, 0 (a) and 3 nm (b), and (ii) a hemispherical cap with a radius of 1 nm.

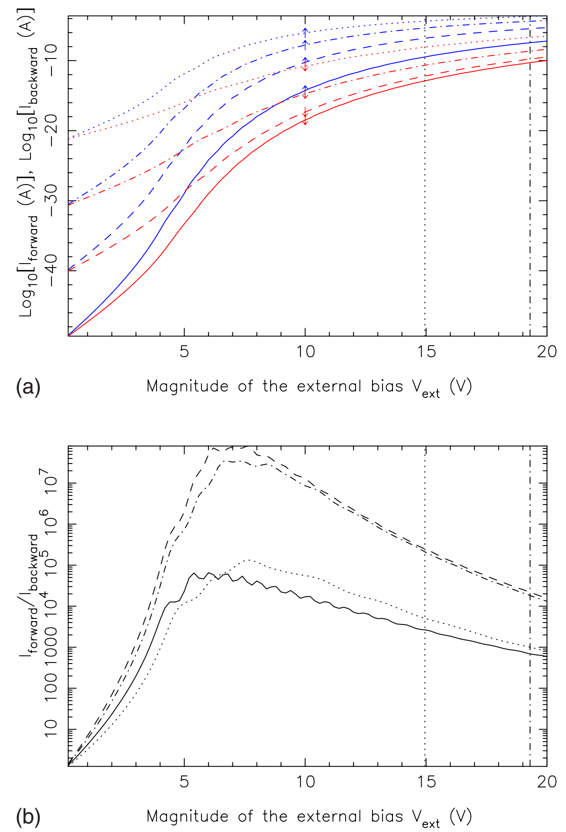


FIG. 9. (Color online) (a) Forward (curves indicated by an upward arrow) and backward (curves indicated by a downward arrow) currents as a function of the magnitude of the external bias $V_{ext}$. (b) Rectification ratio of the junction as a function of the magnitude of the external bias $V_{ext}$. The bottom metal supports a protrusion that consists of (i) a cylindrical body with a radius of 1 nm and a height of, respectively, 0 (solid), 1 (dashed), 2 (dot-dashed), and 3 nm (dotted), and (ii) a hemispherical cap with a radius of 1 nm. The spacing $D$ between the two metals is 6 nm. The vertical lines indicate the voltage at which the tunneling part of the barrier, for electrons propagating along the $z$ axis at the Fermi level of the bottom metal, disappears.

apex of the tip and the top metal. This reduction results indeed in a stronger field on the top metal, which enhances the backward current. This effect becomes negligible as $D \to \infty$.

The right part of Fig. 9 reveals that the highest rectification ratio is achieved when the height of the protrusion is 2 nm. It was seen indeed that both the forward and backward currents increase with the height of the tip. The ratio between these two quantities finds its optimum at the height value of 2 nm. Below this turning point, the increase of the forward bias is faster than the increase of the backward current. The rectification ratio increases therefore with the height of the tip. Above this turning point, it is the backward current that increases more rapidly than the forward current. The rectification ratio is therefore decreasing. This increase of the backward current will become less significant at larger spacing values, so that the rectification ratio will find its optimal value at higher protrusion heights. In the limit where $D \to \infty$, increasing the protrusion height will only impact the forward current and increase both the rectification ratio and the mean power the junction can provide to an external load.

For a given bias, the mean power is higher with the 4 nm protrusion. With the 14.9 V voltage at which the tunneling part of the surface barrier disappears (for the 4 nm protrusion), the power $\langle P \rangle$ is $3.4 \times 10^{-4}$ W (cutoff frequency of 0.3 THz). The forward current and the mean power one obtains with the other protrusions are smaller. With the 3 nm protrusion, the bias at which the tunneling part of the barrier disappears is 19.3 V. The mean power one obtains in these conditions is $4.2 \times 10^{-4}$ W (cutoff frequency of 0.2 THz). The maximal current and thus the mean power one can obtain with the different protrusions are of the same order of magnitude. The higher protrusions have the advantage that

lower fields are required in order to reach these maximal values.

## V. CONCLUSIONS

In this paper, we have studied metal-vacuum-metal junctions in which the lower metal supports a hemispherical protrusion. Because of this geometrical asymmetry, the system exhibits rectification properties that were examined in detail by using a transfer-matrix methodology, which specifically takes account of three-dimensional aspects of the potential barrier. In particular, we studied how these rectification properties depend on the external bias, on the separation between the two metals, on differences in the work function and temperature, and on the height of the protrusion. These results demonstrate in a more quantitative way that junctions presenting either a geometrical, a material, or a thermal asymmetry exhibit rectification properties, which enable the production of dc currents from an oscillating field. Systems similar to those considered in this paper could therefore be used as an energy converter, with the energy extracted from the oscillating field being transferred through this dc current into an external circuit. The response time of the device is limited by the tunneling process, whose characteristic time is of the order of a femtosecond. The classical propagation time that follows the tunneling process limits the cutoff frequency of the rectification to values situated in either the visible spectrum or in the infrared. Our simulations confirm that rectification in the visible spectrum can be achieved, in principle, provided the spacing between the two electrodes is sufficiently small, so that electrons can transit through the device before the bias produced by incident radiation reverses. It is known that replacing the vacuum by an oxide layer increases the mechanical stability of the device structure. However this replacement could increase the cutoff frequency only for conditions where the drift velocity of electrons in the oxide would be larger than the average velocity obtained in vacuum. Although materials with high electron mobilities can be found,[32] the buildup of surface charges and the dielectric constant of these materials limit dramatically the internal fields and thus the drift velocities one can achieve. A detailed analysis of this more complex situation goes beyond the scope of this paper, but our previous work indicates that surface charges can screen the external field by many orders of magnitude,[33] so that this condition of higher drift velocities would, in general, not be met.

## ACKNOWLEDGMENTS

A.M. is funded as a research associate by the National Fund for Scientific Research (FNRS) of Belgium. The authors acknowledge the use of the Interuniversity Scientific Computing Facility (ISCF) of Namur. A.A. Lucas is acknowledged for encouraging comments and valuable suggestions.

*Corresponding author; alexandre.mayer@fundp.ac.be

[1] T. E. Sullivan, P. H. Cutler, and A. A. Lucas, Surf. Sci. **54**, 561 (1976).
[2] K. H. Evenson, G. W. Day, J. S. Wells, and L. O. Mullen, Appl. Phys. Lett. **20**, 133 (1972).
[3] W. Krieger, T. Suzuki, M. Volcker, and H. Walther, Phys. Rev. B **41**, 10229 (1990).
[4] N. M. Miskovsky, S. H. Park, P. H. Cutler, and T. E. Sullivan, J. Vac. Sci. Technol. B **12**, 2148 (1994).
[5] K. M. Evenson, J. S. Well, F. R. Peterson, B. L. Danielson, G. W. Day, R. L. Barger, and J. L. Hall, Phys. Rev. Lett. **29**, 1346 (1972).
[6] *Proceedings of the 17th General Conference on Measures and Weights, Sevres, France* (Comptes Rendus, BIPM, 1983), p. 93.
[7] P. Gueret, A. Baratoff, and E. Marclay, Europhys. Lett. **3**, 367 (1987).
[8] P. H. Cutler, T. E. Feuchtwang, T. T. Tsong, H. Nguyen, and A. A. Lucas, Phys. Rev. B **35**, 7774 (1987).
[9] H. Q. Nguyen, P. H. Cutler, T. E. Feuchtwang, Z.-H. Huang, Y. Kuk, P. J. Silverman, A. A. Lucas, and T. E. Sullivan, IEEE Trans. Electron Devices **36**, 2671 (1989).
[10] T. E. Sullivan, Y. Kuk, and P. H. Cutler, IEEE Trans. Electron Devices **36**, 2659 (1989).
[11] T. E. Hartman, J. Appl. Phys. **33**, 3427 (1962).
[12] L. O. Hocker, D. R. Sokoloff, V. Daneu, A. Szoke, and A. Javan, Appl. Phys. Lett. **12**, 401 (1968).
[13] J. F. Mulligan, Am. J. Phys. **44**, 963 (1976).
[14] J. Terrien, Rep. Prog. Phys. **39**, 1067 (1976).
[15] A. A. Lucas, A. Moussiaux, M. Schmeits, and P. H. Cutler, Commun. Phys. (London) **2**, 169-74 (1977).
[16] N. M. Miskovsky, S. J. Shepherd, P. H. Cutler, T. E. Sullivan, and A. A. Lucas, Appl. Phys. Lett. **35**(7), 560-2 (1979).
[17] N. M. Miskovsky, S. J. Shepherd, P. H. Cutler, T. E. Sullivan, and A. A. Lucas, Appl. Phys. Lett. **35**, 560 (1979).
[18] G. Binnig and H. Rohrer, IBM J. Res. Dev. **30**, 355 (1986).
[19] C. Fumeaux, W. Herrmann, F. K. Kneubuhl, and H. Rothuizen, Infrared Phys. Technol. **39**, 123 (1998).
[20] N. Beverini, G. Carelli, E. Ciaramella, G. Contestabile, A. De Michele, and M. Presi, Laser Phys. **15**, 1334 (2005).
[21] E. Bava, N. Beverini, G. Carelli, A. De Michele, G. Galzerano, E. Maccioni, A. Moretti, M. Prevedelli, F. Sorrentino, and C. Svelto, IEEE Trans. Instrum. Meas. **54**, 1407 (2005).
[22] A. Mayer and Ph. Lambin, Nanotechnology **16**, 2685 (2005).
[23] Th. Laloyaux, I. Derycke, J.-P. Vigneron, Ph. Lambin, and A. A. Lucas, Phys. Rev. B **47**, 7508-18 (1993).
[24] A. Mayer and J.-P. Vigneron, Phys. Rev. B **56**, 12599 (1997).
[25] A. Mayer and J.-P. Vigneron, Phys. Rev. E **59**, 4659 (1999).
[26] A. Mayer and J.-P. Vigneron, Phys. Rev. E **60**, 7533 (1999).
[27] A. Mayer and J.-P. Vigneron, Phys. Rev. E **61**, 5953 (2000).
[28] A. Mayer and J.-P. Vigneron, Phys. Rev. B **62**, 16138 (2000).
[29] A. Mayer, N. M. Miskovsky, and P. H. Cutler, Phys. Rev. B **65**, 195416 (2002).

[30] M. Büttiker, Y. Imry, R. Landauer, and S. Pinhas, Phys. Rev. B **31**, 6207 (1985).

[31] R. H. Good and E. W. Müller, in *Handbuch der Physik*, edited by S. Flugge (Springler Verlag, Berlin, 1956), Vol. 21, p. 176.

[32] V. W. L. Chin, T. L. Tansley, and T. Osotchan, J. Appl. Phys. **75**, 7365 (1994).

[33] A. Mayer, N. M. Miskovsky, and P. H. Cutler, Semicond. Sci. Technol. **20**, 202 (2005).